

Fuel consumption assessment of an electrified powertrain with a multi-mode high-efficiency engine in various levels of hybridization

A. Solouk^{a,b,*}, M. Shakiba-Herfeh^b, J. Arora^a, M. Shahbakhti^a

^a Mechanical Engineering-Engineering Mechanics, Michigan Technological University, Houghton, MI 49931, USA

^b Ford Motor Company, Dearborn, MI 48124, USA



ARTICLE INFO

Keywords:

LTC engines
Optimization
Fuel consumption
Parallel HEV
PMP

ABSTRACT

Powertrain electrification including hybridizing advanced combustion engines is a viable cost-effective solution to improve fuel economy of vehicles. This will provide opportunity for narrow-range high-efficiency combustion regimes to be able to operate and consequently improve vehicle's fuel conversion efficiency, compared to conventional hybrid electric vehicles. Low temperature combustion (LTC) engines offer the highest peak brake thermal efficiency (BTE) reported in literature, but these engines have narrow operating ranges. In addition, LTC engines have ultra-low soot and nitrogen oxides (NOx) emissions, compared to conventional compression ignition and spark ignition (SI) engines. In this study, an experimentally developed multi-mode LTC-SI engine is integrated into a parallel hybrid electric configuration, where the engine operation modes include homogeneous charge compression ignition (HCCI), reactivity controlled compression ignition (RCCI), and conventional SI. The powertrain controller is designed to enable switching among different modes, with minimum fuel penalty for transient engine operations. A pontryagin's minimum principal (PMP) methodology is used in the energy management supervisory controller to study a multi-mode LTC engine in parallel HEV architecture with various hybridization levels. The amount of torque assist by the e-motor can change the LTC mode operating time, which leads to variation in the vehicle's fuel consumption. The results for the urban dynamometer driving schedule (UDDS) driving cycle show the maximum benefit of the multi-mode LTC-SI engine is realized in the mild electrification level, where the LTC mode operating time increases dramatically from 5.0% in a plug-in hybrid electric vehicle (PHEV) to 20.5% in a mild HEV.

1. Introduction

The U.S. light-duty (LD) regulations require a fleet average of 4.3 l/100 km by 2025 in order to meet the 101 g/km CO₂ level [1]. In addition, in the European Union, the average fleet fuel consumption regulations for the new cars require 4.1 l/100 km by 2021 [2]. High efficiency engines along with powertrain electrification will play a critical role in meeting such stringent goals from the cost-effectiveness perspective [3–5]. Currently, the spark-ignition (SI) engine fueled with gasoline is the primary engine used in the LD vehicles in the U.S. [1]. Conventional compression ignition (CI) engines are noteworthy for the LD vehicles due to their higher efficiency. However, the CI engines require an expensive and complex aftertreatment system for particulate matter (PM) and NO_x control [6]. To improve vehicular fuel economy and reduce aftertreatment expenses, various studies have investigated advanced combustion regimes to achieve higher thermal efficiencies than those in CI engines while mitigating engine-out emissions [7–9]. A promising advanced combustion regime is low temperature combustion

(LTC), and consists of a family of variants including homogeneous charge compression ignition (HCCI), reactivity controlled compression ignition (RCCI), and partially-premixed charge compression ignition (PCCI) [10,11]. LTC engines can offer peak indicated thermal efficiency of 53% [9] with ultra low NO_x and PM engine-out emissions [9]. Even though the LTC engines benefit from higher thermal efficiencies and less expensive after treatment systems compared to conventional engines, they have narrow operating ranges and often require more complex combustion control which makes them challenging for application in automotive powertrains. As the fleet merges to a higher degree of powertrain electrification path, more opportunities for advanced combustion regimes (i.e., LTC) will arise. It is because the powertrain electrification allows the engine to be downsized and operated in a narrow-range high-efficiency combustion regimes as compared to the conventional powertrains.

Fig. 1 catagorizes the prior hybrid electric vehicle (HEV) studies based on different engine types including conventional (i.e., SI, CI, Atkinson) and advanced combustion (i.e., LTC) engines. In the first

* Corresponding author at: Ford Motor Company, Dearborn, MI 48124, USA.

E-mail addresses: asoloukm@mtu.edu (A. Solouk), mshakiba@ford.com (M. Shakiba-Herfeh), jkarora@mtu.edu (J. Arora), mahdish@mtu.edu (M. Shahbakhti).

Nomenclature	
<i>Abbreviations</i>	
BSFC	brake specific fuel consumption
BTE	brake thermal efficiency
EVC	exhaust valve closing
HEV	hybrid electric vehicle
HCCI	homogeneous charge compression ignition
HWFET	highway fuel economy test
ICE	internal combustion engine
IVO	intake valve opening
LD	light duty
LTC	low temperature combustion
LVD	longitudinal vehicle dynamic
OCV	open circuit voltage
PMP	Pontryagin's minimum principle
PHEV	plug-in hybrid electric vehicle
RCCI	reactivity controlled compression ignition
RON	research octane number
SOC	state of charge
SI	spark ignition
UDDS	urban dynamometer driving schedule
<i>Symbols</i>	
λ	co-state [–]
C_d	vehicle aerodynamic drag coefficient [–]
\dot{m}_f	fuel consumption rate [g/sec]
f_r	rolling resistance coefficient [–]
ω	engine speed [rpm]
ω_{motor}	E-motor speed [rpm]
A	vehicle frontal area [m^2]
\mathcal{H}	Hamiltonian [g/sec]
M	vehicle total mass [kg]
n_c	mechanical coupling ration [–]
n_t	transmission ratio [–]
n_d	differential ratio [–]
$P_{motor,mech}$	traction mechanical power of e-motor [kW]
$P_{motor,e}$	Regen electrical power of e-motor [kW]
P_{bat}	battery power [kW]
P_{wheel}	power demand at wheel [kW]
P_{eng}	engine generated power [kW]
Q_{nom}	battery nominal energy capacity [Wh]
R	battery internal resistance [Ω]
V_{veh}	vehicle speed [$\frac{m}{sec}$]
r	wheel radius [m]
ρ	air density [$\frac{kg}{m^3}$]
θ	road slope [°]
m_{ij}	mode-switching fuel penalty [g]
u	control variable
<i>Subscripts</i>	
bat	battery
$drag$	drag
eng	engine
e	electrical
$grade$	gradeability
$gear$	gearbox
$intake$	intake
min	minimum
max	maximum
$motor$	electric motor
$mech$	mechanical
nom	nominal
veh	vehicle
$roll$	rolling resistance

category, conventional SI and CI engines have been used in different HEV architectures. The SI engines have been integrated in HEV and range extender architectures [12–18]. Atkinson SI engines are popular in the market and are used in the Toyota Prius, Ford C-Max, Lexus RX 450 h, and Honda Accord. In Refs. [19,20], Toyota has achieved 10% lower fuel consumption compared to SI engine by converting the Honda Accords PHEV SI engine to the Atkinson cycle. The CI engines mostly have been integrated in trucks and sport utility vehicles (SUVs) [21–25].

In the second category, the LTC engines are integrated in different HEV architectures. Few studies are found in the literature that explores the LTC-HEV powertrain. Such powertrains are divided into two sub-categories based on the LTC combustion regimes including the single-mode LTC and multi-mode LTC. In majority of the previous works, the engine has been flexible to switch from a single-mode LTC to a conventional mode [5,26–28], while in [29] we carried out the first study of integrating a multi-mode LTC engine in HEVs. Thus, the engine not only could switch to conventional modes, but also it could switch among different LTC modes. In the single-LTC mode subcategory, HCCI was the first type that was studied in electrified powertrains. In the first study at the United States Argonne National Laboratory, the effects of using a dual-mode SI-HCCI engine in different vehicle electrification levels were analyzed [27]. In both studies, in Ref. [26,28], the fuel economy benefits of the SI-HCCI engine are studied for parallel HEV architectures. In [30], we carried out the first study by utilizing a pure HCCI mode engine in a series hybrid powertrain and we found 12.6% improvement in fuel economy in comparison with a series HEV running with an SI engine over a combined US driving cycle consisting of UDDS,

HWFET, and US06 cycles. In our next study [31], we investigated the impact of driving cycles, number of the engine operating points, and engine startup fuel penalty on both series HEV and extender range electric vehicle HCCI-based powertrains. RCCI was the second type of LTC engine that was studied in an HEV powertrain. In Ref. [32], researchers at the University of Wisconsin-Madison and Oak Ridge National Laboratory used an RCCI engine in a series-parallel hybrid electric powertrain and they found 12% fuel economy improvement over the similar HEV running with a modern SI engine in the HWFET driving cycle. In Ref. [33] we found 3% fuel economy improvement over diesel engine in a series HEV architecture by using an RCCI engine in the US06 driving cycle. In [5] the RCCI-CI engine is integrated in a power-split HEV architecture in which a rule-based energy management controller (EMC) was used for evaluating the fuel economy improvement.

Moreover, in [34] a multi-mode LTC engine was designed to switch between the HCCI, RCCI and conventional SI modes in a series HEV architecture. The results showed a 9.1–12.1% fuel economy improvement, compared to an identical series HEV platform running with a single-mode SI engine over the HWFET driving cycle. In [35] a multi-mode LTC engine was utilized in a torque-blended HEV architecture and preliminary optimization results were presented.

Building upon our previous works in [34,35], this paper presents the first study undertaken to investigate the fuel economy benefit of integrating a multi-mode LTC-SI engine with a parallel HEV with an advanced optimal control strategy, and incorporating measured fuel penalty map for mode switching and including constraints for required exhaust gas temperature to enable high conversion efficiency for

Engine Type and Combustion Strategy		
	Conventional	LTC
Controller Types Rule-Based, Global Optimization (DP, Pontryagin's Minimum Principle), and Real Time (MPC, ECMS, SDP)	<p>SI</p> <ul style="list-style-type: none"> MPC Control of Parallel HEV [Rezaei 2015] PMP Control of Parallel PHEV [Triboli 2014] RBC and PMP Control of Range Extenders [Sciarretta 2014] DP Controller in Parallel HEV [Kum 2011] Online EMC of PHEV, SHEV, and S/P-HEV [Kessels 2008] <p>Atkinson</p> <ul style="list-style-type: none"> Engine Sizing for a PHEV [Yonekawa 2013] Engine Designing for a Parallel HEV [Kawamoto 2009] <p>CI</p> <ul style="list-style-type: none"> Optimization based EMC for Series Plug-In Bus [Hu 2013] MPC Control of a Series-Parallel [Kermani 2012] SDP Control of a Series-Parallel [Opila 2012] ECMS Control of a Parallel HEV [Sciarretta 2004] <p>DP Control of a Series HEV [Brahma 2000]</p>	<p>Single-Mode LTC</p> <p>HCCI</p> <ul style="list-style-type: none"> RBC of SI-HCCI Different HEVs [Delorme 2010] RBC of Dual Mode SI-HCCI S/P HEV in [Lawler 2011] ECMS of S/P HEV in Dual Mode SI-HCCI [Ahn 2012] RBC, DP, and MPC in Series HEV/ Range Extender [Solouk 2015] <p>RCCI</p> <ul style="list-style-type: none"> Manually Tuned, Fixed Engine Power in a Series HEV [Hanson, 2015] Rule-based EMC in Power-Split RCCI-Diesel Engine [Gao 2015] DP and MPC based EMC with Variable Engine Power in Series HEV [Solouk 2016b] <p>Multi-Mode LTC</p> <p>Series HEV</p> <ul style="list-style-type: none"> Preliminary Optimization [Solouk 2016a] Comprehensive Optimization Including Measured Mode-Switching Fuel Penalty, NVH Constraint and Exhaust Emission Catalyst Light-Off Temperature Constraints [Solouk 2017b] <p>Torque-Blended</p> <ul style="list-style-type: none"> Preliminary Optimization [Solouk 2017a] Comprehensive Optimization Including Measured Mode-Switching Fuel Penalty and Exhaust Emission Catalyst Light-Off Temperature Constraints [This Work]

Fig. 1. Different types of ICEs and control techniques used in HEVs in previous studies.

exhaust aftertreatment systems. The LTC modes in this work include both HCCI and RCCI modes that are applied for a 2-4 cylinder engine.

The major contributions of this paper are:

- It determines the potential for fuel consumption reduction of a multi-mode EV-LTC-SI powertrain in a “P2 parallel HEV” configuration, including realistic constraints for implementing the proposed powertrain.
- It specifies and incorporates experimental constraints including (1) catalyst light-off temperature via including exhaust gas temperature constraints and (2) measured mode switching fuel penalty in HEV optimization framework.

- It examines the effect of different electrification levels on the fuel consumption of the multi-mode EV-LTC-SI parallel HEV.

This paper is organized in five sections. In the following section, the HEV experimental setup is explained. Next, the optimal control problem for a parallel HEV architecture is formulated and pontryagin's minimum principle (PMP) optimization techniques are applied. Then, the results of the parallel HEV for the single-mode and multi-mode engine operations are discussed. Finally, all findings from this paper are summarized in the last section and conclusions are drawn.

2. Electrified multi-mode LTC-SI engine experimental setup

This section overviews the experimental setup that is designed and built at Michigan Technological University for this study. This experimental setup enables testing LTC engine hybridization to investigate different aspects of the LTC-HEV powertrain. The setup is comprised of a fuel-flexible 2.0-l LTC-SI engine and a 100-kW electric powertrain, which are connected to a 465 hp double-ended AC dynamometer. Fig. 2 shows the experimental setup in this study. The fuel-flexible LTC engine can be adapted to operate in different LTC modes including HCCI, RCCI and also conventional SI mode. Operating conditions for each of these three engine modes are listed in Table 2. The electric powertrain is capable of realizing different levels of powertrain electrification.

Details on the experimental setup are found in Ref. [34]. Here, a brief overview of the experimental setup is provided.

2.1. Multi-mode engine setup

The baseline engine setup includes a GM 2.0-l Ecotec Gasoline Direct Injection Turbocharged SI engine. Table 1 lists the engine specifications. The baseline SI engine was converted to a multi-mode LTC-SI engine, in which the LTC modes include HCCI and RCCI. Major changes to the baseline SI engine include (i) design of control strategies and programming new engine control unit (ECU), (ii) adding port fuel injection systems, and (iii) capability to adjust intake charge temperature, pressure, and dilution level through utilizing intake air heater, supercharger, and exhaust gas recirculation (EGR) rate modulation, respectively.

Engine control units included dSPACE® MicroAutoBox (MABx) DS1511 and RapidPro units. Models for control of cam phasers, fuel pump, injectors, spark plugs, supercharger, throttle body, and EGR valve were developed in Simulink®. These models were compiled into a single engine control program, and related parameters were monitored and controlled in real-time using the dSPACE ControlDesk®. The ACAP® system was used as the combustion analyzer and the in-cylinder pressures were measured using PCB 115A04 piezo electric pressure transducers. Experiments were performed for three different combustion modes, namely SI, HCCI, and RCCI.

Two fuel rails were installed at the interface of the intake manifold and cylinders for port fuel injection. A low-pressure external fuel pump was used to supply fuel at 3 bar pressure to the port fuel injectors and a high-pressure fuel pump was used to supply fuel at 100 bar pressure to direct fuel injectors. The injection system has the capability of

Table 1
Parameters of the baseline engine in this study.

Parameters	Value/Description
Engine model	GM Ecotec LHU
Bore × Stroke	86 × 86 mm
Number of cylinders	4
Displacement volume	2.0 L
Compression ratio	9.2:1
Connecting rod length	145.5 mm
Max power	270 hp @6000 rpm
Fuel injection system	Gasoline direct injection
Valve system	DOHC 4 valves

supplying three fuels to the engine at the same time. The amount of fuel injected was controlled using dSPACE® MABx. Pressures (coolant, oil, and intake air) and temperatures (exhaust gas, intake air, coolant and oil gallery) were measured using piezo resistive pressure transducers with an accuracy of 0.5% and K-type thermocouples with an accuracy of 0.75%, respectively. The mass flow rate of intake air was measured using Merriam MDT500 air flow measurement system. The engine speed and load were controlled using a 465 hp General Electric AC dynamometer.

Operating conditions such as intake air temperature (T_{intake}), intake manifold pressure (P_{intake}), research octane number (RON) of fuel, engine speed (N), and equivalence ratio (ϕ) were varied individually keeping the other parameters constant. The operating conditions used for each of the combustion modes are given in Table 2. The experiments were conducted for a range of engine speeds and a range of equivalence ratios between the knock and misfire limits. Thereby, the operating region and load limit for each combination of input parameters were determined.

Using the data acquired from dSPACE®, LabVIEW® and ACAP®, the combustion and performance parameters were calculated using an in-house Matlab® code. The brake specific fuel consumption (BSFC) maps were generated and the load limits for each of the combustion modes were determined. Fig. 3 shows the BSFC maps for SI, HCCI and RCCI combustion modes with engine speed (RPM) on the x-axis and engine brake torque (N m) on the y-axis. The valve timing is set to provide the best brake thermal efficiency. In the process of developing the experimental engine maps, the control variables were tuned to ensure the engine operating points are knock free and have low NOx emissions. For instance, start of injection for DI was adjusted to ensure knock-free operation and stable combustion $COV_{IMEP} \leq 3\%$. The EGR was not used

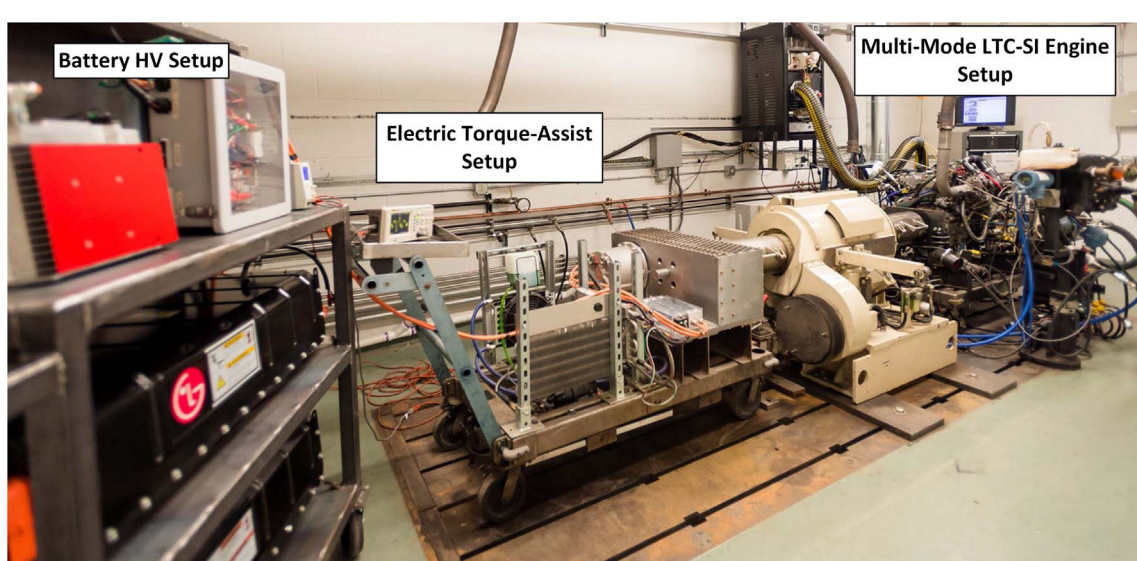


Fig. 2. Developed LTC-based hybrid electric powertrain experimental testbed with a double-ended 465 hp AC dynamometer at Michigan Technological University.

Table 2

Engine test setting for SI and LTC operating modes.

Combustion mode	SI	HCCI	RCCI
Fuel injection system	DI	PFI1 + PFI2	DI + PFI1
Fuel type	Gasoline/iso-octane	n-heptane + iso-octane	n-heptane + iso-octane
Engine speed (rpm)	800–4000	800–1600	800–2200
SOI (CAD bTDC)	100	450	Variable
IVO (CAD bTDC)	−24.5	25.5	25.5
EVC (CAD bTDC)	22	22	22
T _{intake} (°C)	40	40, 60, 80, 100	40, 40, 80, 100
P _{intake} (kPa)	100	100	100
RON (−)	87	0–40	20–60

in the data points presented in the maps.

The measured exhaust gas temperatures are shown in Fig. 4 for SI, RCCI, and HCCI operating modes. The SI engine exhaust gas temperature ranges from 457 °C to 776 °C. This temperature range changes to 246–660 °C, and 200–442 °C for the RCCI and HCCI operating modes, respectively. Given CO and HC conversion efficiency in the exhaust catalytic converter is a function of the catalyst temperature, the engine operating points are selected to meet the minimum catalyst light-off temperature (i.e., 300 °C [36]). This is realized by considering the engine exhaust gas temperature as a constraint in the optimization framework, which will be discussed in Section 3.

As part of this study, the aim was to develop a multi-mode engine which can utilize either HCCI, RCCI or SI mode. This allows the engine to utilize the high thermal efficiency of LTC modes at lower to mid loads, while using high thermal efficiency points of the SI mode at full load range. To this end, mode switching control strategies among SI and LTC modes were developed – see Refs. [34,37] for details. Fig. 5 illustrates the resulted fuel penalty values for both RCCI to SI and SI to HCCI switches in different engine speeds and torques. The mode switchings between the different engine modes are bidirectional.

A switch to the SI mode is needed at the point where either SI mode

is more efficient compared to LTC modes or LTC combustion is not possible. Optimum combustion phasing and load were set for the SI mode by tuning the throttle position, fuel quantity and spark timing. Similarly, for the RCCI mode, start of injection (SOI) and premixed ratio (PR) were adjusted. The tuned steady state points for each mode were fed as a feedforward command. As soon as the switch was activated, the actuators including throttle, fuel injectors and cam phasors, were varied to attain the required set-point.

For achieving SI to RCCI switch without any misfires, spark assist was provided for 2–3 engine cycles after the switch was activated. This aids auto-ignition of the air-fuel mixture in the RCCI mode. For RCCI to SI switch, to avoid the mixture from becoming too lean while the air condition stabilizes, a strategy for injecting extra fuel was devised. When switching to SI mode, all the fuel came from PFI rail. To compensate for the delay in PFI fueling and air stabilization, direct injection fueling was kept active for 1 cycle after the switch.

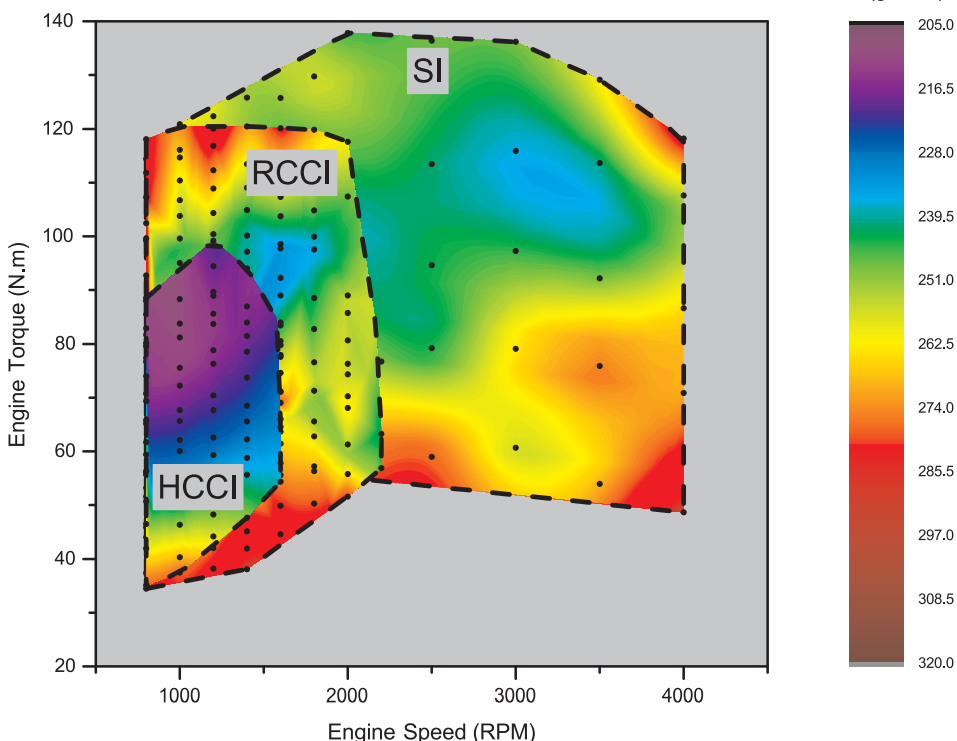
A similar strategy was taken for HCCI-SI switching. In this case, SI was done utilizing DI rail where as PFI rails were utilized for HCCI. Owing to this, the strategy was reversed; that was, for SI to HCCI switching extra fuel was injected. For HCCI to SI, the spark supported switch was carried out.

2.2. Electrified torque-blended setup

The electric powertrain setup includes a 100 kW synchronous induction Remy e-motor, an RMS PM100DX inverter, a 5 kWh/65 kW lithium-ion LG Chem battery, and a mechanical coupling to integrate the motor to the dynamometer (see Table 3). The mechanical drivetrain, including the e-motor mount, coupling, and shafts, were designed and manufactured at Michigan Technological University. The high voltage battery during the operation was connected to the e-motor through a designed pre-charge circuit. The MABx was used as a supervisory controller to monitor sub-level controllers (i.e., battery, e-motor, etc.). The MABx communicated control commands on the CAN bus to the sub-level controllers. The LG Chem battery temperature was controlled through a fan and all the cooling systems were controlled by

BSFC (g/kWh)

Fig. 3. Experimental BSFC map of the developed multi-mode LTC-SI engine. Data points are shown by dot symbols.



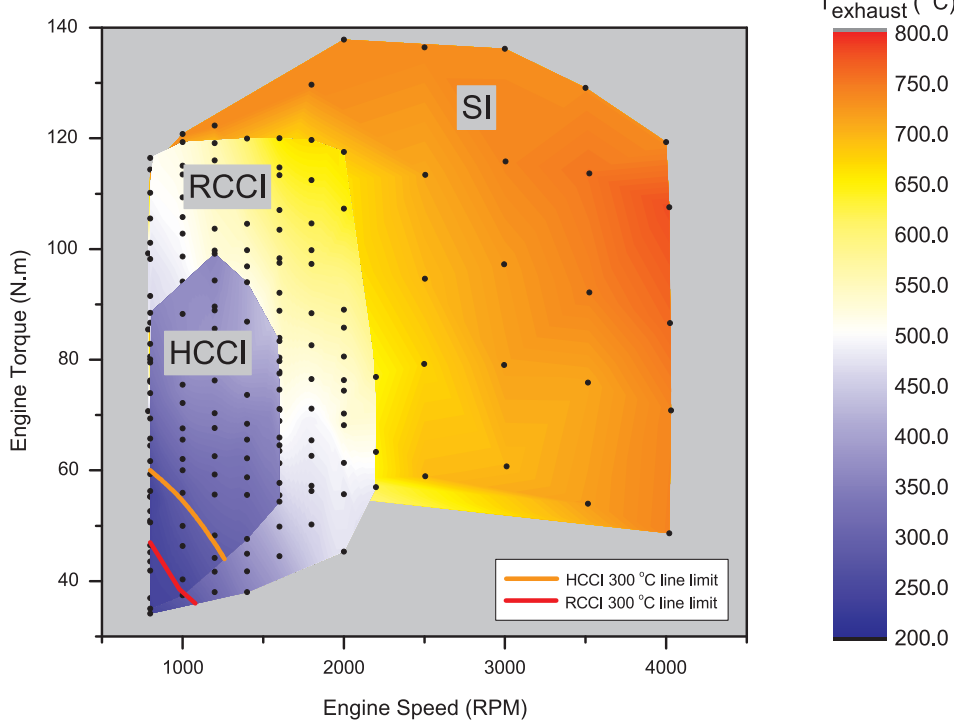


Fig. 4. Experimental temperature map of the developed multi-mode LTC-SI engine. Data points are shown by dot symbols.

the supervisory controller. A fault-action module was developed in Matlab® to manage the setup during faults and extreme conditions.

The driver-commanded torque was carried out through a desired torque-based control strategy embedded in the inverter. The driver's desired speed setpoint was controlled by the dyno controller. The inverter controlled the e-motor to track the reference torque, which was determined by the operator through dSPACE ControlDesk® interface. The e-motor was tested at different load and speed conditions to determine the electric powertrain efficiency maps. These maps are then used in the design of model-based supervisory control strategies.

Fig. 6 shows the e-motor efficiency map that was experimentally calculated using the data in this study by testing e-motor at a range of

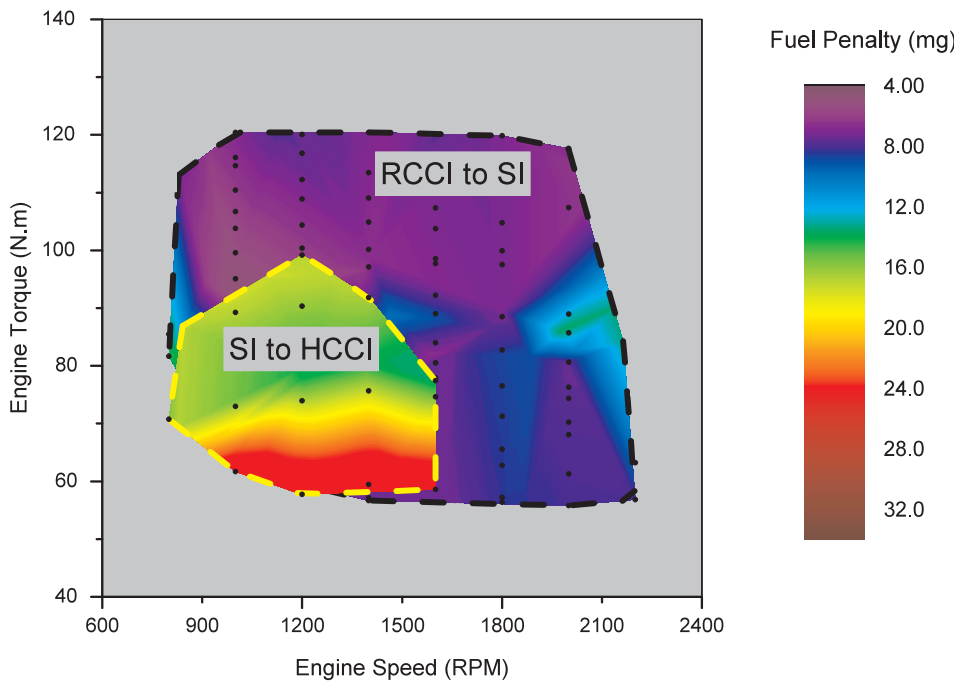


Fig. 5. Experimental mode-switching fuel penalty map.

speeds and torques. The data was collected at the e-motor temperature of 45 °C and the DC voltage of 360 V. Under these conditions, the e-motor efficiency ranges from 71.7% to 91.2%.

In the next section, optimal energy management strategy is designed and implemented for the parallel HEV model with the experimentally validated components using the collected data from the powertrain experimental setup.

3. Design of optimal energy management control strategy

The goal of the optimal control in this study is to minimize the total energy consumption provided by the battery and fuel. In this study the

Table 3

Battery, E-motor, and Inverter specifications used in the experimental setup.

Items	Values
Battery energy capacity (kWh)	5
Battery maximum voltage (V)	410
Battery nominal voltage (V)	360
Battery minimum voltage (V)	260
Battery SOC operating range (%)	30–70
Battery pack mass (kg)	90
E-motor model	HVH250-090-SOM
E-motor DC bus voltage maximum (V)	700
E-motor peak current (Arms)	300
E-motor rated peak operating time (sec)	60
E-motor mass (kg)	49
E-motor rotational inertia ($\text{kg}\cdot\text{m}^2$)	0.067
Inverter maximum DC voltage continuous operating (V)	360
Inverter maximum DC voltage non-continuous operating (V)	500
Inverter peak current limit (Arms)	350
Inverter DC bus capacitor (μF)	440
Inverter mass (kg)	7.5

charge-sustaining mode is considered to provide a fair comparison among different powertrain modes when evaluating fuel saving. Given the battery total energy will be zero in the charge-sustaining mode, the cost function is defined as the total vehicle fuel consumption (\dot{m}_f) by Eq. (1):

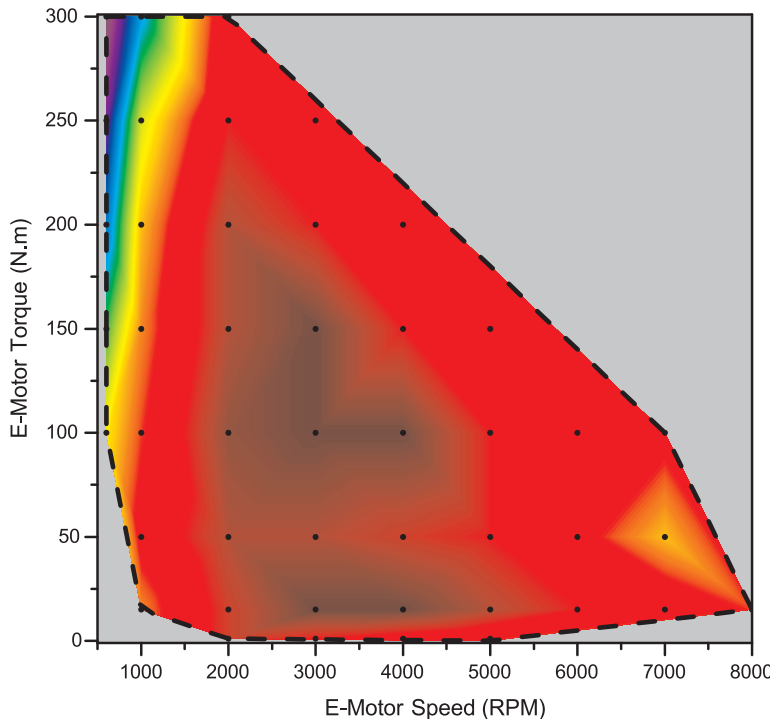
$$J(u(t)) = \int_0^T \dot{m}_f(t) dt \quad (1)$$

where \dot{m}_f is the rate of the engine fuel consumption and T is the time length of a driving cycle. Eq. (2) shows the constraints for the HEV optimization problem.

$$|SOC_f - SOC_0| \leq \epsilon \quad (2a)$$

$$SOC_{min} \leq SOC(t) \leq SOC_{max} \quad (2b)$$

$$P_{bat,min}(SOC) \leq P_{bat}(t) \leq P_{bat,max}(SOC) \quad (2c)$$



$$T_{eng,min}(\omega_{eng}) \leq T_{eng}(t, \omega_{eng}) \leq T_{eng,max}(\omega_{eng}) \quad (2d)$$

$$\omega_{eng,min} \leq \omega_{eng}(t) \leq \omega_{eng,max} \quad (2e)$$

$$T_{motor,min}(\omega_{mot}) \leq T_{motor}(t) \leq T_{motor,max}(\omega_{mot}) \quad (2f)$$

$$\omega_{motor,min} \leq \omega_{motor}(t) \leq \omega_{motor,max} \quad (2g)$$

$$Temp_{exh}(\omega_{eng}, T_{eng}) \geq Temp_{light-off} \quad (2h)$$

The constraints in Eq. (2) are applied for the battery SOC operation window, battery power (P_{bat}), engine torque (T_{eng}), engine speed (ω_{eng}), e-motor torque (T_{motor}), e-motor speed (ω_{motor}), and oxidation catalyst light-off temperature ($Temp_{light-off}$) in the exhaust aftertreatment system. This optimal control problem is solved using optimal control techniques that are described in the following.

3.1. Pontryagin's minimum principle (PMP)

The PMP method is based on a general case of the Euler-Lagrange equation and originates from the calculus of variations. This method yields the necessary - not sufficient - conditions of the global optimal solution. The optimal trajectories derived from PMP will be the global optimal solution of the HEV problem if the obtained optimal trajectory is a unique trajectory that meets the necessary and boundary conditions [38]. The necessary condition for the PMP global optimality is explained in [38] and will be briefly explained in Section 3.1.2. In Sub-Section 3.1.1, the simulation model of the target vehicle is described.

3.1.1. Parallel P2 architecture model

In the P2 parallel HEV architecture, the engine is coupled to the e-motor through a clutch. The output shaft is connected to the drivetrain where an automatic six speed transmission connects the output shaft to the wheels. This limits the engine operating points to discrete gear ratio options. Fig. 7 shows the parallel HEV architecture and Table 4 lists the vehicle parameters along with the transmission ratios used in this study. The operating maps and model parameters for the vehicle components are obtained from the experimental setup as explained in the Section 2.

In the parallel HEV in this work, there are four independent control

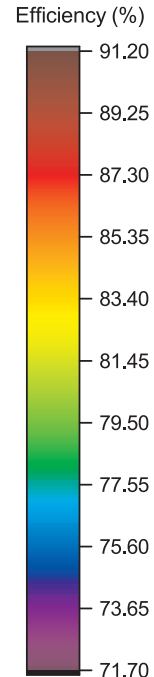


Fig. 6. Combined calculated efficiency map including efficiency of the synchronous PMSM Remy motor and transaxle mechanical losses. Test conditions: e-motor temperature = 45 °C and DC bus voltage = 360 V.

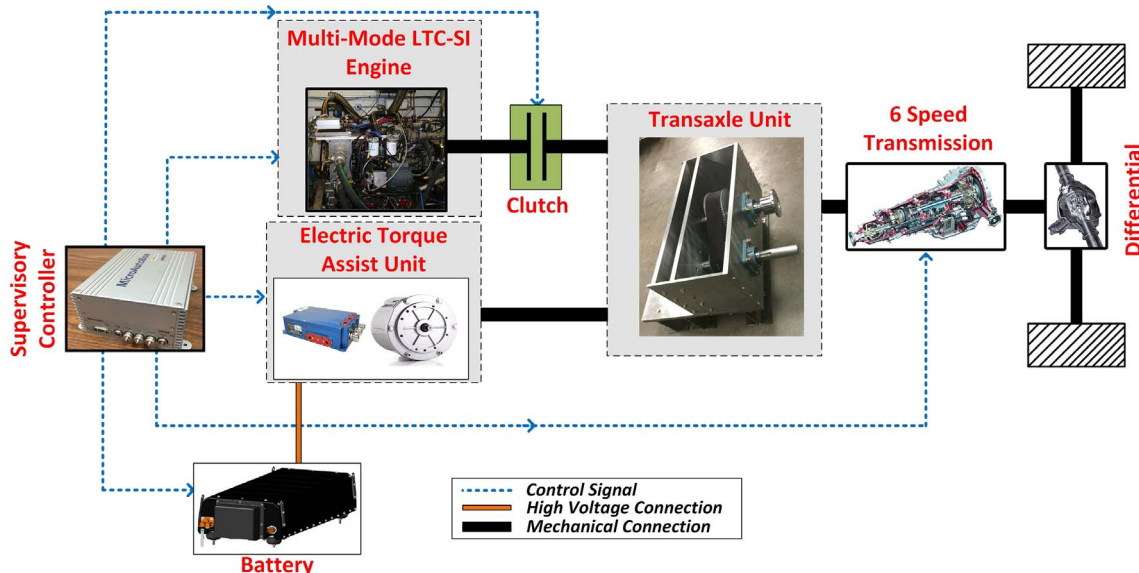


Fig. 7. Parallel HEV architecture in this study.

Table 4
Vehicle specifications.

Parameters	Values
Vehicle curb mass, M	1775 (kg)
Frontal area, A	2.0 (m^2)
Engine motor coupling gear ratio, n_c	2.0 (-)
6-Speed transmission gear ratios	[3.166, 2.05, 1.481, 1.166, 0.916, 0.725] (-)
Differential ratio, n_d	4.529 (-)
Wheel radius, r	0.33 (m)
Drag coefficient, C_d	0.25 (-)
Rolling resistance coefficient, f_r	0.01 (-)

variables. These variables include the engine torque, the battery power, the transmission gear ratio, and the clutch status for a given driver's power request and vehicle speed, as shown in Fig. 8. Both the engine and e-motor speeds can be obtained for a given transmission gear ratio and vehicle speed. The e-motor and engine speeds are determined by Eq. (3), as a function of the vehicle's speed and the transmission gear ratios as follows:

$$\begin{cases} \omega_{motor} = \frac{V_{veh} \cdot n_t \cdot n_d}{r} \\ \omega_{eng} = \frac{\omega_{motor}}{n_c} \end{cases} \quad (3)$$

where V_{veh} is the vehicle speed, n_t is the transmission gear ratio, n_d is the differential ratio, r is the wheel radius, and n_c is the engine/e-motor coupling ratio. The power demand at the wheel is calculated from the longitudinal vehicle dynamics (LVD) model. The purpose of the LVD model is to calculate the vehicle actual speed (V_{veh}) based on vehicle dynamics:

$$MV_{veh} \frac{dV_{veh}}{dt} = P_{wheel} - P_{roll} - P_{drag} - P_{grade} \quad (4)$$

where M is the vehicle total mass; P_{drag} , P_{roll} , and P_{grade} are aerodynamic drag, rolling resistance and gravity powers, respectively. These parasitic powers are calculated by:

$$P_{roll} = Mgf_r \left(1 + \frac{V_{veh}}{100} \right) V_{veh} \quad (5)$$

$$P_{drag} = \frac{1}{2} \rho A C_d V_{veh}^3 \quad (6)$$

$$P_{grade} = MV_{veh} g \sin \theta \quad (7)$$

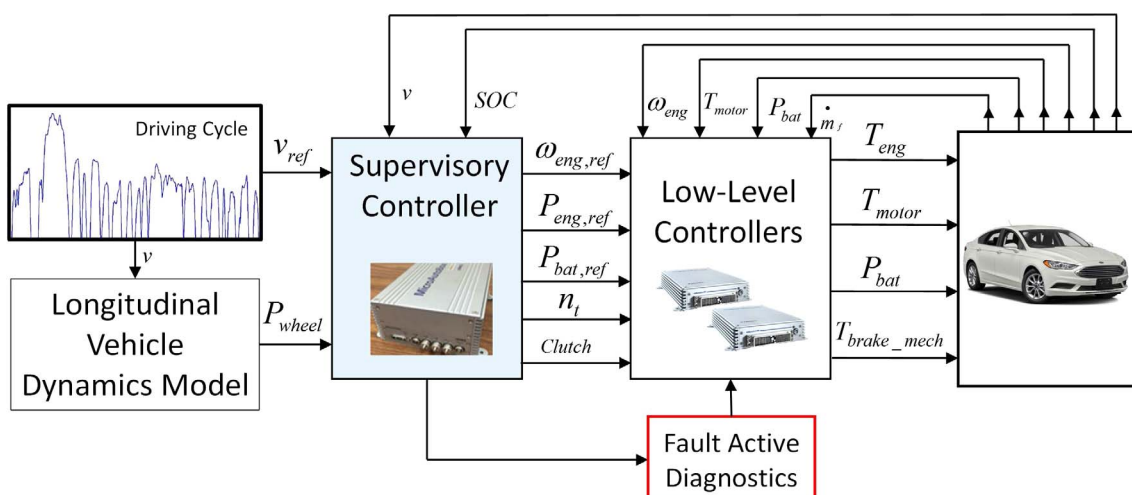


Fig. 8. Supervisory controller schematic block diagram.

Table 5
Definition of hybridization levels in this study.

Hybridization	$\frac{P_{bat}}{P_{eng}}$	Electric motor power (kW)	Operating voltage (V)
PHEV	1.0	60	270–410
Full hybrid	0.65	40	180–270
Mild hybrid	0.30	18	80–120

where ρ is the air density, A is the vehicle frontal area, C_d is the vehicle aerodynamic drag coefficient, f_r is the rolling resistance coefficient, and θ is the road slope. Friction and road conditions will change the P_{wheel}

which is one of the inputs to the energy management control strategy (Fig. 8). Friction will increase driveline loss; thus, the engine or battery is required to provide higher power demand to compensate for the friction loss. Similarly, the road condition (e.g., wet road, dry, etc.) will affect the friction coefficient in the power demand equation (Eq. (5)), which will change the power demand and subsequently the engine operating points. The study in Ref. [39] explores the importance of friction loss in the optimization problem.

In addition, for a given driver's power request, the required engine power can be calculated by Eq. (8) to meet the driver's demand.

$$P_{eng} = P_{wheel} - P_{motor,mech} \quad (8)$$

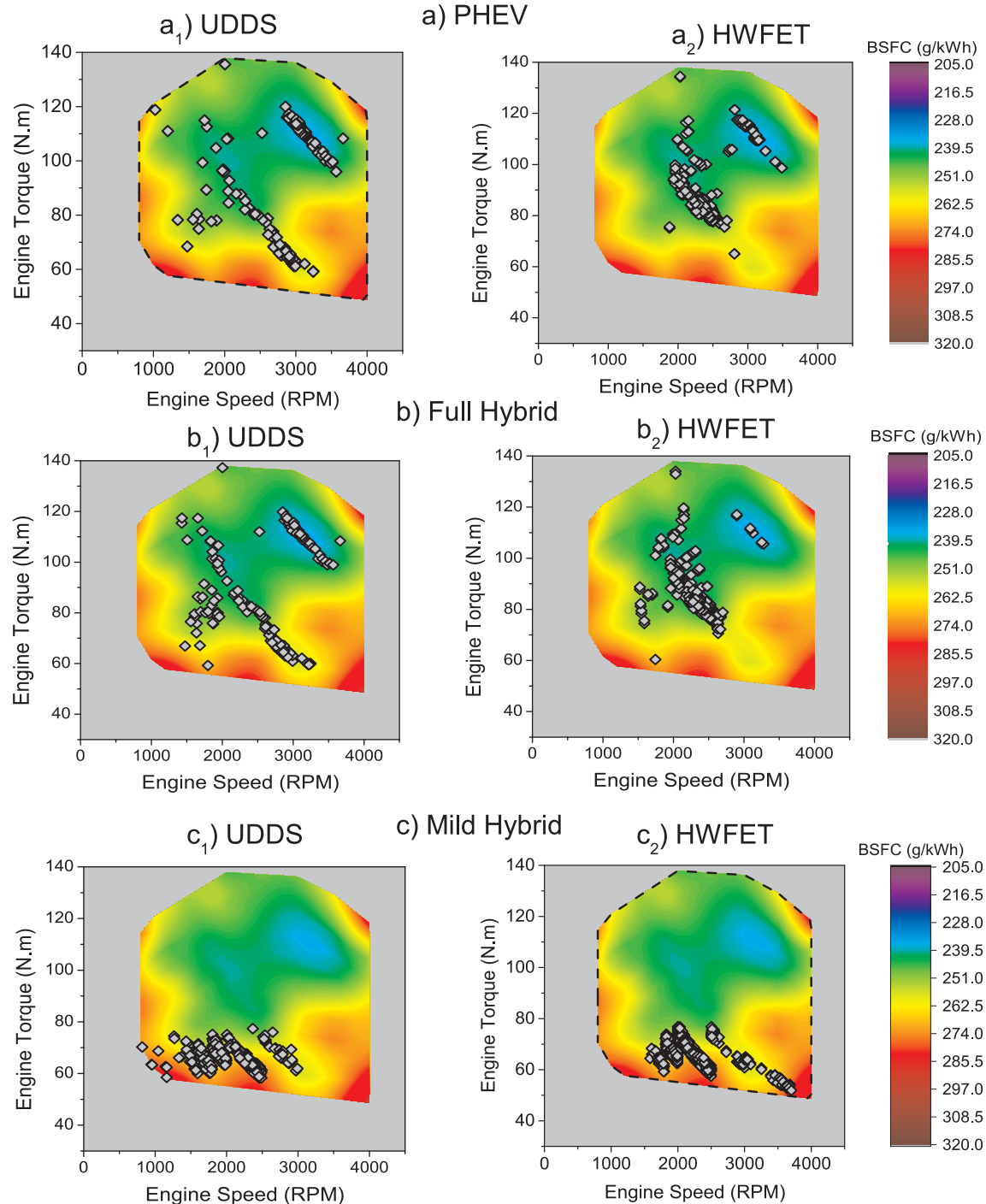


Fig. 9. Engine operating points over the Single-mode engine BSFC map for different electrification levels, (a) PHEV, (b) Full Hybrid, and (c) Mild Hybrid in UDDS and HWFET driving cycles.

Table 6

Results for both multi-mode LTC-SI and single-mode SI engine in different electrification levels during UDDS driving cycle.

Metrics	Multi-mode LTC-SI			Single-mode SI		
	PHEV	Full hybrid	Mild hybrid	PHEV	Full hybrid	Mild hybrid
Fuel consumption (g)	356.3	344.5	378.9	365.5	358.2	409.8
CO ₂ emission (g)	1000	967	1063	1026	996	1120
Ave. engine BTE (%)	34.0	34.3	33.0	33.8	33.6	31.4
Engine work (MJ)	4.80	4.67	5.01	4.90	4.90	5.05
Engine ON time (sec)	233	259	451	184	198	385
Battery loss (kJ)	582	397	307	623	452	352

where $P_{motor,mech}$ is the e-motor mechanical power. Since the battery is supplying the e-motor power, the $P_{motor,mech}$ can be obtained by knowing the battery power and the e-motor efficiency as follows:

$$\begin{cases} P_{bat} = P_{motor,e} \\ P_{motor,mech} = \frac{P_{motor,e}}{(\eta_{motor})^k \cdot \eta_{gear}} \end{cases} \quad (9)$$

where $P_{motor,e}$ is the e-motor input (electrical) power; η_{motor} and η_{gear} are the e-motor and the transmission efficiencies, respectively. k equals to “−1” when the wheel power is positive and equals to “1” when the power at the wheel is negative. The wheel power is determined by the LVD equations.

From Eqs. (3)–(9), the engine power, motor power, engine speed, and motor speeds are specified by knowing the transmission gear ratio (n_t) and the battery power at each time. The motor and engine torques are determined accordingly.

$$\begin{cases} T_{motor} = \frac{P_{motor,mech}}{\omega_{motor}} \\ T_{eng} = \frac{P_{eng}}{\omega_{eng}} \end{cases} \quad (10)$$

The fuel consumption rate is determined from the engine BSFC map as a function of T_{eng} and ω_{eng} :

$$\dot{m}_f = f(T_{eng}, \omega_{eng}) \quad (11)$$

Finally, the time derivative of SOC is obtained from the battery dynamic equation as follows:

$$\dot{SOC}(t) = -\frac{1}{Q_{nom}} \cdot \frac{OCV^2 - \sqrt{OCV^2 - 4R}P_{bat}(t)}{2R} \quad (12)$$

where Q_{nom} is the battery nominal energy capacity. The equivalent open-circuit voltage (OCV) and internal resistance (R) are functions of SOC. Thus, the \dot{SOC} is a function of P_{bat} and SOC. In conclusion, the \dot{m}_f in Eq. (11) and \dot{SOC} in Eq. (12) depend on P_{bat} , and n_t , if the wheel power (P_{wheel}) and vehicle speed are given. Moreover, the P_{bat} , and n_t are selected as the control variables in the optimization problem.

Table 7

Results for both multi-mode LTC-SI and single-mode SI engine in different electrification levels during HWFET driving cycle.

Metrics	Multi-mode LTC-SI			Single-mode SI		
	PHEV	Full hybrid	Mild hybrid	PHEV	Full hybrid	Mild hybrid
Fuel consumption (g)	1168.0	1184.3	1207.2	1170.2	1192.9	1216.0
CO ₂ emission (g)	3324	3418	3517	3366	3443	3542
Ave. engine BTE (%)	34.5	34.2	31.7	34.2	34.1	31.4
Engine work (MJ)	16.1	16.4	15.6	16.2	16.5	15.7
Engine ON time (sec)	850	818	1084	739	798	1052
Battery loss (kJ)	785	717	432	792	770	519

3.1.2. Development of PMP-based torque management strategy

To apply the optimal control theory to the HEV powertrain, the Hamiltonian (\mathcal{H}) is defined as follows:

$$\mathcal{H}(P_{bat}, SOC, t) = -\lambda(t) \cdot g(P_{bat}(t), SOC(t)) + \dot{m}_f(P_{bat}, n_t, t) \quad (13)$$

where λ is called “costate” in the PMP and g is the state equation, which encompasses the battery dynamics (Eq. (12)). Thus, to calculate the Hamiltonian, first the \dot{m}_f and g are determined using control variables, P_{bat} , and n_t from Eqs. (3)–(12).

Using the PMP optimization technique, the state equation and costate equation are obtained as:

$$\dot{SOC} = \frac{\partial \mathcal{H}}{\partial \lambda} \quad (14)$$

$$\dot{\lambda} = \frac{\partial \mathcal{H}}{\partial SOC} \quad (15)$$

From Eqs. (13) and (15), if g is not a function of SOC then the costate can be considered constant, as explained in the following.

In Ref. [29], it is shown that the battery OCV and battery resistance R do not vary significantly in the charge-sustaining over the battery SOC range, i.e. from 0.3 to 0.7. In that case, the costate stays near the initial value since the $\frac{\partial g}{\partial SOC}$ is negligible, compared to the costate for the whole driving cycle. Thus, the costate expression during the SOC usage window is simplified as:

$$\dot{\lambda} = \lambda \frac{\partial g}{\partial SOC} = 0, \quad \rightarrow \lambda = \text{constant} \quad (16)$$

Obtaining a constant value for the costate reduces the PMP complexity. For optimality, the following condition should be considered to specify the optimal control variable P_{bat} and n_t at each time step:

$$\mathcal{H}(P_{bat}^*, n_t^*, SOC^*, \lambda^*, t) \leq \mathcal{H}(P_{bat}, n_t, SOC, \lambda, t) \quad (17)$$

which means that the optimal control variables P_{bat}^* and n_t^* minimize the Hamiltonian function at the given time. The boundary condition of the final state variable is

$$SOC(t_0) = SOC(t_f) \quad (18)$$

The P_{bat}^* , n_t^* , and λ^* that satisfy Eq. (17) and the boundary condition (18), determine the optimal P_{bat} and n_t trajectory. If a costate (λ) exists that fulfills the condition (18), then the PMP provides the ‘global optimal’ solution [38].

3.1.3. Extending the cost function for multi-mode operation

The cost function in Eq. (1) is revised by including the engine startup, LTC-SI mode-switching, and gear shifting fuel penalties for minimizing the number of engine starts, LTC-SI mode-switching, and gear-shifting. The revised cost function (J) is:

$$J(u(t)) = \int_0^T (\dot{m}_f(P_{bat}, t) + \Gamma \cdot F_{p_1} + \Lambda \cdot m_{ij} + \Psi \cdot F_{p_2}) dt \quad (19)$$

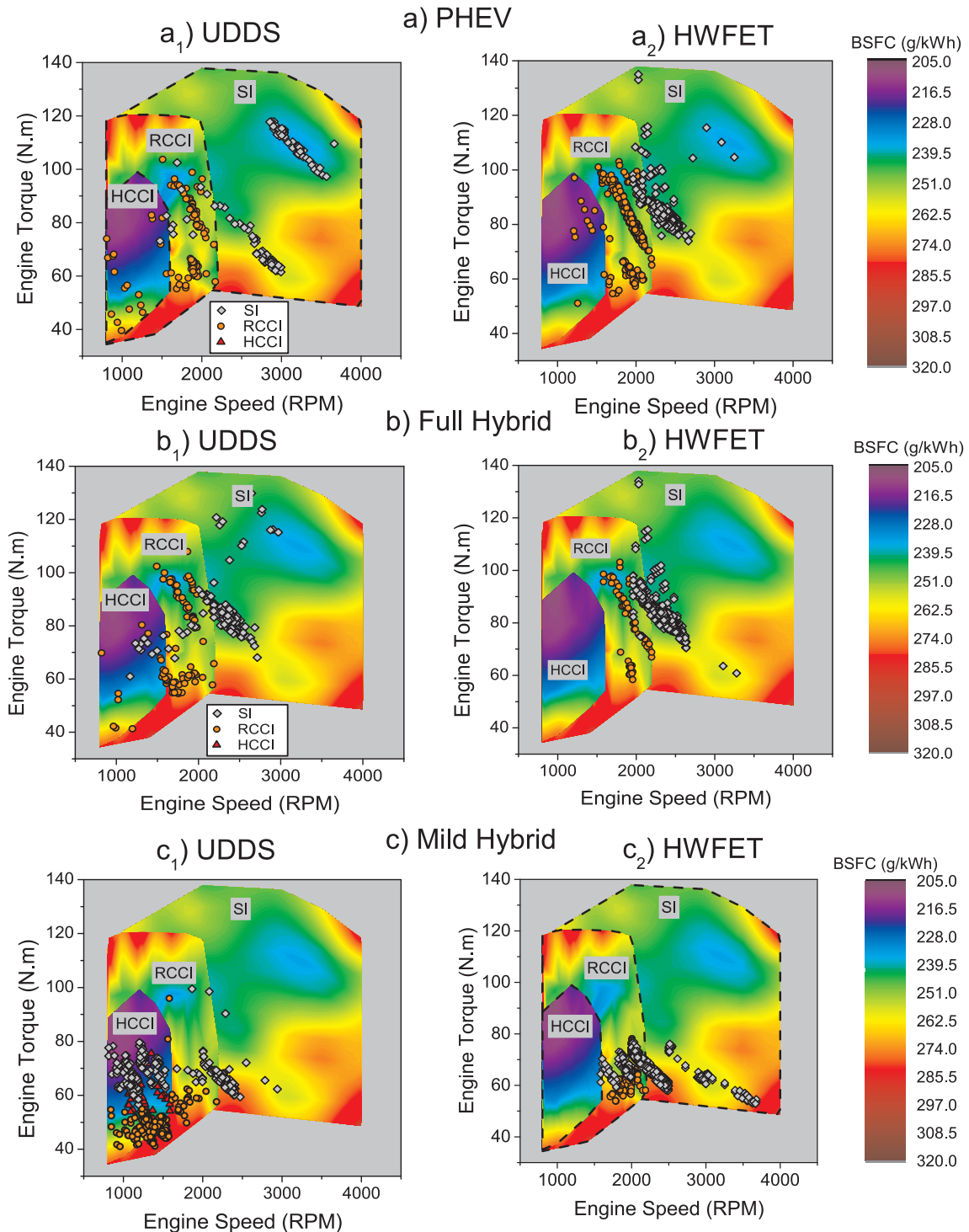


Fig. 10. Engine operating points over the Multi-mode engine BSFC map for different electrification levels, (a) PHEV, (b) Full Hybrid, and (c) Mild Hybrid in UDDS and HWFET driving cycles.

$$\Gamma = \begin{cases} 1, & \text{if } \omega_{eng}(t-1) = 0 \text{ and } T_{eng}(t-1) = 0 \\ & \text{and } T_{eng}(t) \geq \min(T_{eng}(t)) \\ 0, & \text{if } T_{eng}(t) \leq \min(T_{eng}(t)) \end{cases} \quad (20)$$

where Γ determines the condition for adding the engine startup fuel penalty. Λ is zero when the engine is forced to operate in the single-mode regions and Λ is “1” when the mode-switching is allowed. The engine startup fuel penalty F_{p_1} is measured 0.15 g using the data from the experimental setup in Section 2. The F_{p_2} is the fuel penalty to avoid frequent gear shifting ($F_{p_2} = 0.1$ g). Ψ is 1 when $n_t(t) \neq n_t(t-1)$ and Ψ

is zero when $n_t(t) = n_t(t-1)$.

The m_{ij} is mode-switching fuel penalty to switch from the i th engine mode to the j th engine mode. i & $j \in [1,2,3]$, since the engine can run in HCCI, RCCI, and SI modes. The m_{ij} prevents frequent model-switching between different modes. It accounts for the fuel penalty associated with each mode switching and finds the global optimal solution. The m_{ij} in this study is determined by using the experimental fuel penalty map (Fig. 5).

The constraints for the optimal control problem are revised based on the components in the powertrain experimental setup in this study:

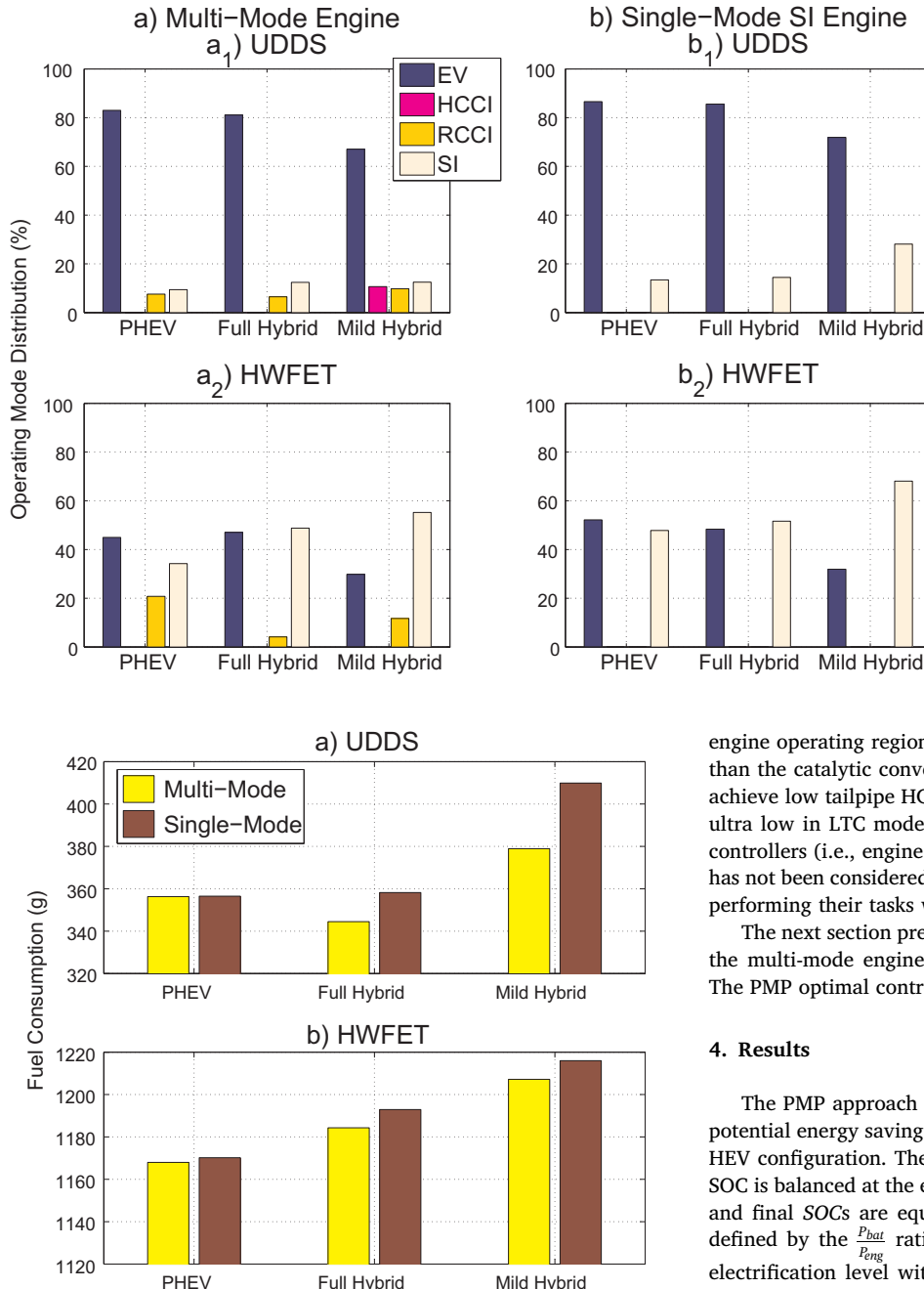


Fig. 12. Fuel consumption for the multi-mode and single mode engines in two driving cycles and three electrification levels.

$$|SOC_f - SOC_0| \leq 0.01 \quad (21a)$$

$$0.3 \leq SOC(t) \leq 0.7 \quad (21b)$$

$$P_{bat,min} \leq P_{bat}(t) \leq P_{bat,max} \quad (21c)$$

$$P_{eng,min}(\omega_{eng}) \leq P_{eng}(t, \omega_{eng}) \leq P_{eng,max}(\omega_{eng}) \quad (21d)$$

$$\omega_{eng,min} \leq \omega_{eng}(t) \leq \omega_{eng,max} \quad (21e)$$

$$0 \leq P_{motor}(t) \leq 100kW \quad (21f)$$

$$0 \leq \omega_{motor}(t) \leq 8000RPM \quad (21g)$$

$$Temp_{exh}(\omega_{eng,min}, T_{eng,min}) \geq 300^\circ C \quad (21h)$$

where a constraint of maximum one percent ΔSOC variation is considered for the charge-sustaining mode. The controller selects the

engine operating regions where the exhaust gas temperature is greater than the catalytic converter light-off temperature (i.e., $300^\circ C$ [36]) to achieve low tailpipe HC and CO emissions. NO_x and soot emissions are ultra low in LTC modes [10]. In this work the effect of the low-level controllers (i.e., engine controller, battery controller, etc.) on the EMC has not been considered. It is assumed that the low-level controllers are performing their tasks without any malfunctions.

The next section presents the results for the single-mode engine and the multi-mode engine integrated with the parallel HEV powertrain. The PMP optimal control solution is used for the analysis in this work.

4. Results

The PMP approach explained in Section 3 is utilized to investigate potential energy saving in the multi-mode LTC-SI engine in the parallel HEV configuration. The costate λ in the PMP is selected such that the SOC is balanced at the end of the driving cycle, which means the initial and final SOCs are equal. Three different levels of hybridization are defined by the $\frac{P_{bat}}{P_{eng}}$ ratio, as listed in Table 5. PHEV has the highest electrification level with peak 60 kW e-motor power and peak 410 V battery voltage. The battery and e-motor power limit in the full hybrid category is defined as 40 kW; this number reduces to 18 kW for the mild hybrid.

Fig. 9 shows the single-mode SI engine BSFC map along with the engine operating points at two hybridization levels. The engine optimum operating points are shown for the Urban Dynamometer Driving Schedule (UDDS) and Highway Fuel Economy Test (HWFET) driving cycles. In both UDDS and HWFET driving cycles, the high power engine operating points are located in the low BSFC region (i.e., $BSFC < 240 \text{ g/kWh}$) for the PHEV, while the engine operating points shift to the low torque and high BSFC regions (i.e., $BSFC > 260 \text{ g/kWh}$) when the hybridization level decreases to mild hybrid category. In addition, in the mild hybrid, the engine operating points are more dependent on wheel speed and power demand since the e-motor assist torque is more limited. This results in less flexibility for the torque management controller to place the engine operating points to the low BSFC region. However, a higher battery and e-motor power in the PHEV provides more flexibility for the hybrid powertrain to shift the engine operating points to the more efficient engine regions, while maintaining the

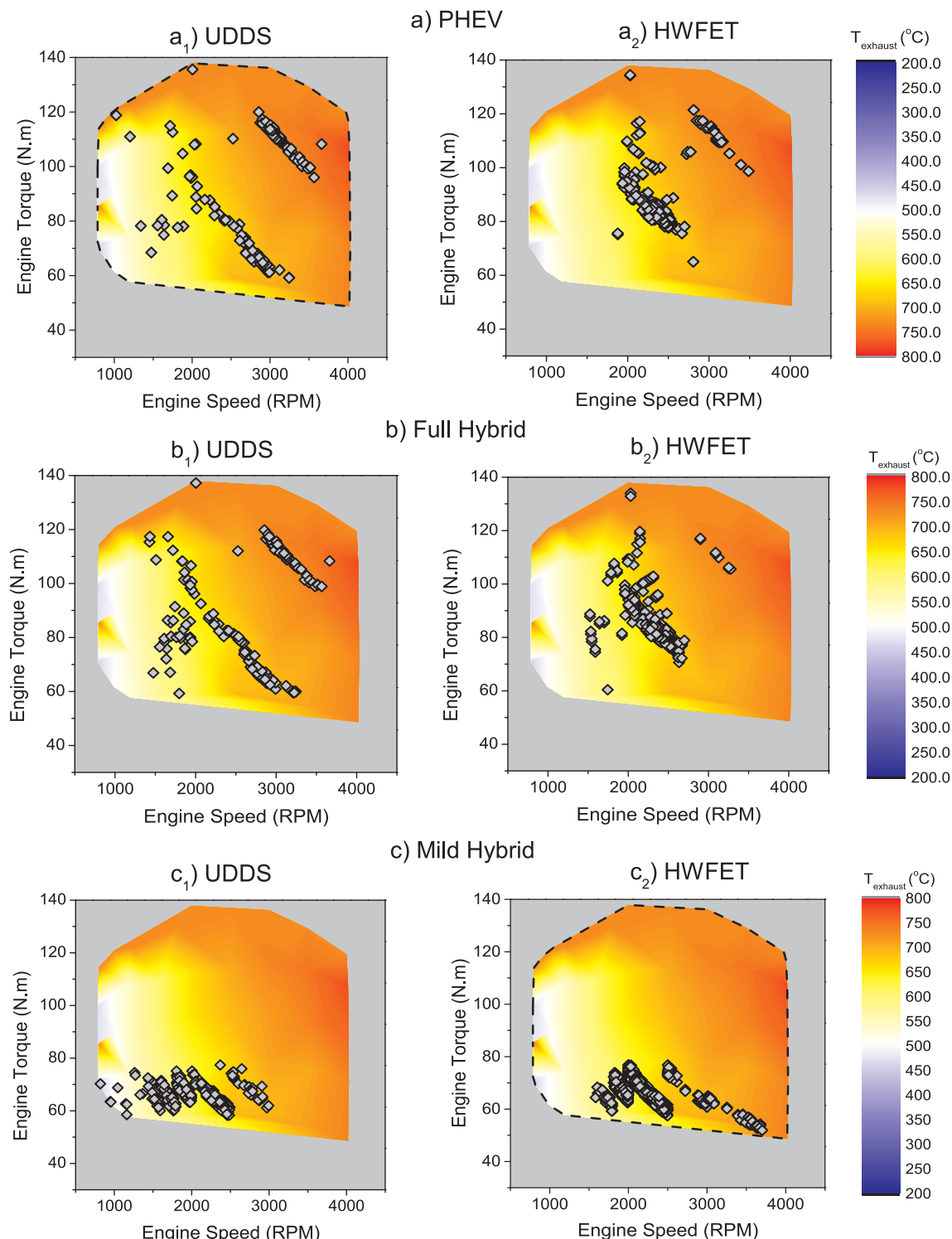


Fig. 13. Engine operating points over the Single-mode engine exhaust gas temperature map for different electrification levels, (a) PHEV, (b) Full Hybrid, and (c) Mild Hybrid in UDDS and HWFET driving cycles.

battery SOC. Hence, the engine ON time, as listed in Table 6, reduces to 184 s in PHEV compared to 385 s in mild hybrid for the UDDS. In the HWFET driving cycle, as listed in Table 7, the engine ON time reduces from 1052 s to 739 s by moving from mild hybrid to PHEV.

Fig. 10 shows the multi-mode LTC-SI engine BSFC map and the engine operating points over the UDDS and HWFET driving cycles. The engine operating points are illustrated for both PHEV and mild hybrid. Comparing Figs. 9-c₁ and 10-c₁ shows that the high BSFC operating points in the single-mode engine are now running in the LTC modes

(i.e., RCCI, HCCI) in the multi-mode engine. Increasing the running time of LTC modes reduces the overall fuel consumption of the vehicle. LTC modes benefit fuel economy in the mild hybrid vehicle over city driving cycle (i.e., UDDS) the most, since it increases the engine brake thermal efficiency (BTE) without charging the battery. In the PHEV, however, the multi-mode LTC-SI engine has less advantage compared to the mild HEV due to availability of higher electric power for locating the engine operating points in high power SI regions with less engine ON time (see Tables 6 and 7). Moreover, in Fig. 10-c₁ the majority of the

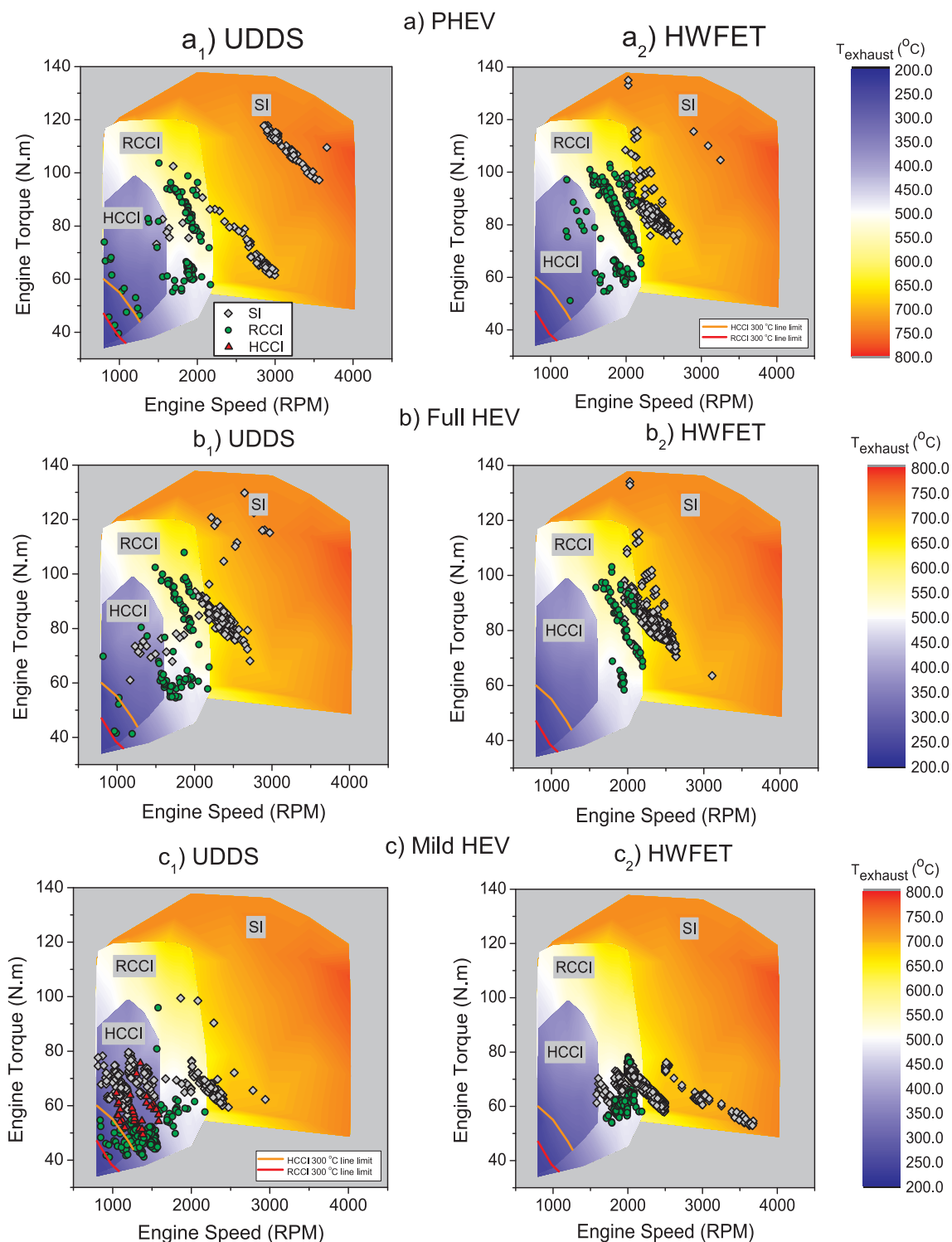


Fig. 14. Engine operating points over the Multi-mode engine exhaust gas temperature map for different electrification levels, (a) PHEV, (b) Full Hybrid, and (c) Mild Hybrid in UDDS and HWFET driving cycles.

engine operating points are in SI mode over the low engine speeds (i.e., 800–1600 rpm) and mid engine torques (i.e., 60–80 N m), while the engine could operate in HCCI mode with a lower BSFC. The optimizer decided to keep the engine on the SI mode in that region due to higher SI-HCCI mode-switching fuel penalty (see Fig. 5). In addition, in Fig. 11-a₁ it can be seen that the engine running time in LTC modes increases by reducing the vehicle electrification level over the UDDS cycle. Among the LTC modes, the RCCI mode has the most engine running time. In parallel P2 architecture, the engine is connected to the

wheels, so selection of the engine operating points at a given wheel power demand and target speed, is limited to the capability of the transmission as well. In this study with the current gear ratios, the optimizer selects the RCCI mode over the HCCI mode. In our previous study, in series architecture [34], the HCCI mode was the dominant engine running mode as the engine operating selection was independent of the wheel load and speed.

A detailed comparison of the engine operating modes in UDDS driving cycle is provided in Table 6. The table shows the fuel

consumption for different hybridization levels along with the engine work and average engine BTE for each case. The mild hybrid multi-mode LTC-SI case shows a 6.3% increase in fuel consumption, compared to the PHEV (note: vehicles were run in charge-sustaining mode). Moreover, in the multi-mode mild hybrid, the engine BTE reduces by 3% and engine work increases by 4.4%, compared to the multi-mode PHEV. Overall, a comparison between the multi-mode LTC-SI and single-mode SI shows that the single-mode SI engine has up to 7.5% higher fuel consumption, 4.9% lower average BTE, and 0.8% more engine work compared to the multi-mode LTC engine. The higher amount of engine work comes from less utilization of e-motor in single-mode SI, which ends up in lower battery loss on discharging and charging the battery. However, the fuel consumption reduction in the multi-mode LTC-SI compared to the single-mode SI reduces from 7.5% to 2.5% by increasing the hybridization level from mild HEV to PHEV.

In addition, [Table 6](#) shows that the engine BTE changes less in the multi-mode LTC-SI engine for different hybridization levels, compared to that in the single-mode SI engine. The relatively lower engine BTE variation (i.e., $\Delta\text{BTE} = 1\%$) in the multi-mode case is due to inherent characteristic of the LTC engines in which the high efficiency region is in the low to mid power area with a small BTE variation. With the high power battery in PHEV, the vehicle has flexibility for placing the engine operating points, independent of wheel power demand. As a result, the engine operating points are placed in low BSFC (i.e., $\text{BSFC} < 233 \text{ g/kWh}$) and high engine power (i.e., $P_{\text{eng}} > 30 \text{ kW}$) regions to provide the propulsion power as well as charging the battery at its maximum capacity. However, in the multi-mode mild hybrid, the engine operating points cannot be placed in the engine high power region since the battery cannot be charged extensively due to its lower power capacity. Moreover, the engine ON time increases by reducing the electrification level. This also links to the less aggressive battery charge/discharge in the mild hybrid compared to the PHEV; thus, the vehicle electric mode decreases and the engine must run for a longer time to provide the demanded power. Note that the larger battery benefits PHEV with capturing greater regens compared to mild/full hybrids. In the multi-mode engine, however, the availability of low BSFC regions enforces the Hamiltonian function to choose the LTC operating modes, whereas in the single-mode the engine has to operate in higher BSFC regions. The advantage of keeping the engine efficiency close to PHEV is pronounced for city cycles such as the UDDS cycle. For highway cycles such as HWFET, since higher wheel power happens at high vehicle speed ($V_{\text{veh}} > 80 \text{ km/h}$), in contrast to city cycles, the HEV controller operates the engine in the best BSFC region of the SI mode with low BSFC values (see [Fig. 10-a}_2](#)). The engine work differences between PHEV and mild hybrid in [Table 6](#) and [Table 7](#) are rooted in missing some regenerative power in the mild hybrid (due to battery power limits). Because of more aggressive battery charging/discharging, in general, the PHEV has more battery loss compared to mild hybrid in the both UDDS and HWFET cycles as it is also listed in [Tables 6](#) and [7](#). Thus, the multi-mode LTC engine benefits are more significant in the mild hybrid compared to the full hybrid and PHEV.

The vehicle fuel consumption is shown in [Fig. 12](#) for both UDDS and HWFET driving cycles. The results show the advantage of the multi-mode LTC-SI engine in the mild hybrid over the single-mode SI. However, this improvement rate is smaller over the HWFET driving cycle since the engine operating points are located mainly in fuel-efficient regions independent of the electrification level.

[Figs. 13 and 14](#) show the engine optimal operating points for single-mode SI and multi-mode LTC-SI engines, respectively over the engine exhaust gas temperature map. All of the engine operating points meet the catalysts light-off temperature constraint (i.e., $T_{\text{exh}} \geq 300^\circ\text{C}$). In [Fig. 14](#) it is shown that even though the engine could operate in the HCCI mode in low engine torque region (i.e., $T_{\text{eng}} < 50 \text{ N m}$) with lower BSFC, instead, it operates in RCCI mode to meet the catalyst light-off temperature constraint. Thus, the powertrain ends up to compromise for lower emissions by losing fuel saving opportunities by running

in RCCI mode compared to running in the HCCI mode.

5. Summary and conclusions

Fuel saving potential of utilizing a multi-mode LTC-SI engine in a parallel HEV in P2 architecture was investigated. The multi-mode engine includes HCCI, RCCI, and SI modes. A hybrid electric setup was designed and built to provide experimental data to develop and validate the HEV model. Optimal energy management strategy is designed and implemented for the parallel HEV model with the experimentally validated components using the collected data from the powertrain experimental setup and analyzed for different hybridization levels. The powertrain controller was designed to enable switching among different modes, while minimizing fuel consumption by including a penalty for transient engine operations. The exhaust gas temperature was included in the optimization framework to minimize the HC and CO tailpipe emissions. Below are the main findings based on the optimization results in this study:

- The results for the UDDS driving cycle show the multi-mode LTC-SI engine offers up to 7.5% fuel saving over a single-mode SI engine in the mild parallel HEV. This improvement reduces to 0.7% for the HWFET driving cycle. This is because, in the highway driving cycle, the high power at wheels happens at high vehicle speeds; therefore, the optimal control strategy forces the engine to run at high engine speeds due to transmission gear limitations. Given the HCCI and RCCI modes cannot be operated at high engine speeds, running the engine at the SI mode for a shorter amount of time was the optimal strategy.
- The engine LTC running time increases from 7.6% to 20.5% by reducing the vehicle electrification level from PHEV to mild HEV, over the UDDS driving cycle. Among the LTC modes, the mid power RCCI with the current transmission selection and mode-switching fuel penalty was the dominant mode that had the most engine running time.
- The engine has less opportunity to operate in the low power region of the HCCI mode by considering the catalyst light-off temperature constraint. Instead, the optimal strategy chooses the RCCI mode as the engine operating mode with the higher exhaust gas temperature, compared to that in the HCCI mode.
- In the parallel multi-mode LTC-SI powertrain, two ways for fuel savings include operating in the LTC mode or using electric torque assist offered by the e-motor. Fuel saving from these two ways are not additive. In strong hybridizations (e.g., PHEV) the optimizer commands to operate the engine in high power region of SI engine and turns off the engine for a longer time, while in mild hybrids, due to lack of sufficient electric power for charge-sustaining, the optimizer cannot locate the engine operating points in high power region, and, instead, the engine operating points shift to lower power regions which happen to be the LTC modes to save fuel.
- Compared to full electrified vehicles such as PHEVs, mild electrified vehicles such as mild HEVs are better suited to improve fuel economy in the multi-mode LTC-SI engine. However, the PHEV provides the lowest fuel consumption among the other electrification levels.

Future work may include the robustness analysis of the developed EMC against the sensor faults, and disturbances like aerodynamic and road roughness as described in Refs. [40,41]. In addition, the transmission design and optimal selection of gear ratios for the P2 parallel hybrid electric powertrain requires further investigations. Finally, the selection of the engine operating points can affect the vibrational dynamics of the vehicle, since the engine speed can be located in the range of the vehicle chassis resonance frequency which can cause ride quality issues. Therefore, by changing the engine operating points, the fuel consumption of the vehicle will be different. This requires further

investigations.

Acknowledgments

This work was partially supported by the United States National Science Foundation under Grant No. 1434273. LG Chem Power Inc. is gratefully acknowledged for providing the battery packs in this study. The authors would like to thank Dr. Seyfi Polat, Dr. Hamit Solmaz, Paul Dice, and Michigan Tech. Energy Mechatronics Laboratory (EML) graduate students who contributed in building the experimental powertrain setup in this study.

References

- [1] United States National Research Council. Cost, effectiveness, and deployment of fuel economy technologies for light-duty vehicles. Washington, DC: The National Academies Press; 2015, doi:<http://dx.doi.org/10.17226/21744>.
- [2] European Commission Climate Action <<https://ec.europa.eu/clima/policies>> [accessed on Nov. 15, 2016].
- [3] Berube M. PHEVs - a transition to the future? In: SAE range extenders for electric vehicles symposium. Knoxville (TN, USA), Nov. 2016.
- [4] Sarkar R. Balancing regulations and customer expectations in future powertrain, fuel, lubricant vehicle systems. In: SAE international powertrains, fuels and lubricants meeting. Baltimore (USA), Oct. 2016.
- [5] Gao Z, Curran SJ, Parks JE, Smith DE, Wagner RM, Daw CS, Edwards KD, Thomas JF, et al. Drive cycle simulation of high efficiency combustions on fuel economy and exhaust properties in light-duty vehicles. *Appl Energy* 2015;157:762–76.
- [6] Johnson TV. Review of diesel emissions and control. *Int J Eng Res* 2009;10(5):275–85.
- [7] Shahbakhti M, Koch CR. Characterizing the cyclic variability of ignition timing in a homogeneous charge compression ignition engine fuelled with n-heptane/iso-octane blend fuels. *Int J Eng Res* 2008;9(5):361–97.
- [8] Curran S, Gao Z, Wagner R. Reactivity controlled compression ignition drive cycle emissions and fuel economy estimations using vehicle systems simulations with E30 and ULSD. *SAE Int J Eng* 2014;7:902–12.
- [9] Reitz R, Duraisamy G. Review of high efficiency and clean reactivity controlled compression ignition (RCCI) combustion in internal combustion engines. *Prog Energy Combust Sci* 2015;46(4):12–71.
- [10] Shahbakhti M, Koch CR. Physics base control oriented model for HCCI combustion timing. *ASME J Dynam Syst, Measur Control* 2010;132(2).
- [11] Nazemi M, Shahbakhti M. Modeling and analysis of fuel injection parameters for combustion and performance of an RCCI engine. *Appl Energy* 2016;165:135–50.
- [12] Rezaei A, Burl JB. Prediction of vehicle velocity for model predictive control. *IFAC-PapersOnLine* 2015;48(15):257–62.
- [13] Rezaei A, Burl JB. Effects of time horizon on model predictive control for hybrid electric vehicles. *IFAC-PapersOnLine* 2015;48(15):252–6.
- [14] Rezaei A, Burl JB, Zhou B. Estimation of the ECMS equivalent factor bounds for hybrid electric vehicles. *IEEE Trans Control Syst Technol* 2017. <http://dx.doi.org/10.1109/TCST.2017.2740836>.
- [15] Sciarretta A, Serrao L, Dewangan PC, Tona P, Bergshoeff E, Bordons C, et al. A control benchmark on the energy management of a plug-in hybrid electric vehicle. *Control Eng Pract* 2014;29:287–98.
- [16] Kum D, Peng H, Bucknor NK. Supervisory control of parallel hybrid electric vehicles for fuel and emission reduction. *J Dynam Syst, Measur, Control* 2011;133(6).
- [17] Rezaei A, Burl JB, Solouk A, Zhou B, Rezaei M, Shahbakhti M. Catch energy saving opportunity (CESO), an instantaneous optimal energy management strategy for series hybrid electric vehicles. *Appl Energy* 2017.
- [18] Zhou B, Burl JB, Rezaei A. Hybrid electric vehicle battery aging estimation and economic analysis based on equivalent consumption minimization strategy. *SAE Paper No.* 2017-01-1251; 2017.
- [19] Yonekawa A, Ueno M, Watanabe O, Ishikawa N. Development of new gasoline engine for ACCORD plug-in hybrid. *SAE Paper No.* 2013-01-1738; 2013.
- [20] Kawamoto N, Naiki K, Kawai T, Shikida T, Tomatsuri M. Development of new 1.8-liter engine for hybrid vehicles. *SAE Paper No.* 2009-01-1961; 2009.
- [21] Hu X, Murgovski N, Johannesson L, Egardt B. Energy efficiency analysis of a series plug-in hybrid electric bus with different energy management strategies and battery sizes. *Appl Energy* 2013;111:1001–9.
- [22] Kermani S, Delprat S, Guerra T, Trigui R, Jeanneret B. Predictive energy management for hybrid vehicle. *Control Eng Pract* 2012;20(4):408–20.
- [23] Opila DF, Wang X, McGee R, Gillespie RB, Cook J, Grizzle JW. An energy management controller to optimally trade off fuel economy and drivability for hybrid vehicles. *IEEE Trans Control Syst Technol* 2012;20(6):1490–506.
- [24] Sciarretta A, Back M, Guzzella L. Optimal control of parallel hybrid electric vehicles. *IEEE Trans Control Syst Technol* 2004;12(3):352–63.
- [25] Brahma A, Guezenne Y, Rizzoni G. Optimal energy management in series hybrid electric vehicles. *Proc Am Control Conf* 2000;1(6):60–4.
- [26] Lawler B, Ortiz-Soto E, Gupta R, Peng H, Filipi Z. Hybrid electric vehicle powertrain and control strategy optimization to maximize the synergy with a gasoline HCCI engine. *SAE Int J Eng* 2011. p. 1115–26.
- [27] Delorme A, Rousseau A, Wallner T, Ortiz-Soto E, Babajimopolous A, Assanis D. Evaluation of homogeneous charge compression ignition (HCCI) engine fuel savings for various electric drive powertrains. In: 25th world battery, hybrid and fuel cell electric vehicle symposium & exhibition; 2010.
- [28] Nüesch S, Stefanopoulou AG. Multimode combustion in a mild hybrid electric vehicle. Part 1: supervisory control. *Control Eng Pract* 2016;57:99–110.
- [29] Solouk A, Shakiba-herfah M, Kannan K, Solmaz H, Dice P, Bidarvatan M, et al. Fuel economy benefits of integrating a multi-mode low temperature combustion (LTC) engine in a series extended range electric powertrain. *SAE Technical Paper No.* 2016-01-2361; 2016.
- [30] Solouk A, Shahbakhti M, Mahjoub MJ. Energy management and control of a hybrid electric vehicle with an integrated low temperature combustion (LTC) engine. In: ASME dynamic systems and control conference (Paper No. DSCC2014-6286). San Antonio (TX, USA), Oct. 2014.
- [31] Solouk A, Shahbakhti M. Modeling and energy management of an HCCI based powertrain for series hybrid and extended range electric vehicles. *Int J Powertrains* 2017;6(2). <http://dx.doi.org/10.1504/IJPT.2017.10001761>.
- [32] Hanson R, Spannbauer S, Gross C, Reitz RD, Curran S, Storey J, et al. Highway fuel economy testing of an RCCI series hybrid vehicle. *SAE Paper No.* 2015-01-0837; 2015.
- [33] Solouk A, Shahbakhti M. Energy optimization and fuel economy investigation of a series hybrid electric vehicle integrated with diesel/RCCI engines. *Energies* 2016;9(12). <http://dx.doi.org/10.3390/en9121020>.
- [34] Solouk A, Tripp J, Shakiba-Herfah M, Shahbakhti M. Fuel consumption assessment of a multi-mode low temperature combustion engine as range extender for an electric vehicle. *Energy Convers Manage* 2017;148(2017):478–1496.
- [35] Solouk A, Shakiba-herfah M, Shahbakhti M. Analysis and control of a torque blended hybrid electric powertrain with a multi-mode LTC-SI engine. In: 2017 SAE world congress, SAE Paper No. 2017-01-1153; 2017.
- [36] Shahbakhti M, Ghazimirsaid A, Koch CR. Experimental study of exhaust temperature variation in a homogeneous charge compression ignition engine. *Proc Inst Mech Eng, Part D: J Autom Eng* 2010;224(9):1177–97.
- [37] Arora JK. Design of real-time combustion feedback system and experimental study of an RCCI engine for control, MSc. Thesis. Michigan Technological University; 2016.
- [38] Kim N, Cha S, Peng H. Optimal control of hybrid electric vehicles based on Pontryagin's minimum principle. *IEEE Trans Control Syst Technol* 2011;19(5):1279–87.
- [39] Wang R, Jing H, Yan F, Karimi HR, Chen N. Optimization and finite-frequency H_{∞} control of active suspensions in in-wheel motor driven electric ground vehicles. *J Frank Inst* 2015;352(2):468–84.
- [40] Kommuri SK, Defoort M, Karimi HR, Veluvolu KC. A robust observer-based sensor fault-tolerant control for PMSM in electric vehicles. *IEEE Trans Indust Electron* 2016;63(12):671–7681.
- [41] Sabrina A, Chadli M, Karimi HR. Robust static output-feedback controller design against sensor failure for vehicle dynamics. *IET Control Theory Appl* 2014;8(9):728–37.